

# LUNISOLAR PERTURBATIONS OF HIGH-ECCENTRICITY ORBITS SUCH AS THE MAGNETOSPHERIC MULTISCALE MISSION

**Trevor Williams<sup>1</sup>, Eric Palmer<sup>2</sup>, Jacob Hollister<sup>2</sup>, Dominic Godine<sup>2</sup>,  
Neil Ottenstein<sup>2</sup> and Rich Burns<sup>3</sup>**

For highly eccentric orbits such as that of the Magnetospheric Multiscale (MMS) mission, with apogee radius now 29.34 Earth radii, the third-body effects of Sun and Moon are the major perturbations. One key consequence is an oscillation in MMS perigee altitude, on an approximately 6 year cycle. This variation has already required perigee-raise maneuvers to avoid an untimely reentry. There is also a long-term evolution in the orientation of the MMS orbit, with period roughly twice as long. This effect may potentially be useful for MMS science studies, as it can bring the spacecraft into new regions of the magnetosphere.

## INTRODUCTION

The NASA Magnetospheric Multiscale (MMS) mission is flying four spinning spacecraft in highly elliptical orbits to study the magnetosphere of the Earth [1]. Launch on an Atlas V 421 occurred from Kennedy Space Center on Mar. 12, 2015, with insertion into a high-eccentricity orbit that was designed to satisfy a complicated set of science and engineering constraints [2]. After roughly 5 months of commissioning, the spacecraft were flown in tetrahedron formations of varying dimensions [3][4] for science data collection. In the first phase of the mission, these measurements were taken on the dayside of the Earth, in a Region of Interest surrounding the apogee of the MMS orbit (radius  $12 R_E$ ). The goal during Phase 1 was to observe the magnetic reconnection events that are expected to occur near the magnetopause, where the solar wind impinges upon the magnetosphere. Measurements during the later Phase 2b, after apogee radius was increased to  $25 R_E$  (roughly two fifths of the way to the Moon) [5], were taken in the magnetotail [6], to similarly observe nightside magnetic reconnection events. Taking simultaneous measurements from four spacecraft allows spatial derivatives of the electric and magnetic fields to be determined, allowing variations that are functions of distance to be distinguished from those that are functions of time. The prime mission was completed successfully in Sept. 2017, and MMS is currently carrying out further science data collection in an extended mission that is expected to be lengthy.

The major perturbation of the MMS orbit at its initial apogee radius of  $12 R_E$  was caused by the oblateness of the Earth: this produced secular drifts in both right ascension of the ascending node and argument of perigee. However, around midway through the campaign to raise apogee radius to  $25 R_E$ , the third-body effects produced by the Sun and Moon [7] became significant. Lunisolar perturbations were by far the major effect at this higher orbit, as they are for the new apogee radius of  $29.34 R_E$  (giving an orbital period of 3.5 days) that was entered into in Feb. 2019. This paper will describe the lunisolar perturbations that have been seen in the past, and are predicted for the future, for these high orbits, discuss the practical implications of these perturbations, and examine to what extent lunisolar effects can be modulated by spacecraft maneuvers.

---

<sup>1</sup> Aerospace Engineer, Navigation and Mission Design Branch, NASA Goddard Space Flight Center, Greenbelt, MD 20771. Associate Fellow, AIAA. Phone: (443)545-4736. Email: [Trevor.W.Williams@nasa.gov](mailto:Trevor.W.Williams@nasa.gov)

<sup>2</sup> Aerospace Engineer, a.i. solutions, Inc.

<sup>3</sup> Project Manager, Space Sciences Mission Operations, NASA Goddard Space Flight Center.

One key consequence of lunisolar perturbations is a strong variation in MMS perigee altitude. It can be seen that perigee evolves with a period of slightly over 6 years: this periodicity is seen for a wide range of variations in the initial conditions of the MMS orbit. A distinction between these various cases, however, is on which cycle reentry will occur: at the  $25 R_E$  apogee radius, this did not occur until 2068, so comprehensively violating the NASA 25-year reentry rule for debris mitigation. By contrast, one of the effects of raising apogee to  $29.34 R_E$  was that reentry was brought forward to 2030. (If desired, a relatively small perigee-raise maneuver can then be used to delay reentry to the next 6-year cycle, i.e. 2036.) It should be noted that reentry for highly eccentric orbits such as that of MMS is much more predictable than for low Earth orbits: reentry will occur when lunisolar effects bring perigee down into the atmosphere. Drag, which is inherently difficult to predict precisely, only participates on essentially the final orbit of the mission. It should also be noted that reentry occurs not as a result of a decrease in semi-major axis, but rather due to an increase in eccentricity. This can be shown to result from changes in the angular momentum of the orbit, which are produced by torques applied by Sun and Moon. The geometry of this type of interaction will be discussed in the paper.

Another significant consequence of lunisolar effects is a long-term evolution in the orientation of the MMS orbit. One aspect of this can be seen by examining the MMS equatorial and ecliptic (more significant for science) inclinations: these can be seen to vary with the same period of slightly over 6 years that was seen for perigee. By contrast with the large changes in inclination that are seen at apogee radii of 25 and  $29.34 R_E$ , equatorial inclination varied by only around 0.3 deg during the two years that MMS spent at its initial  $12 R_E$  apogee radius. Of course though, inclination provides only a partial description of the orbital orientation: when a fuller visualization is examined, a period of about 13 years, or twice the previous roughly 6-year cycle, becomes evident. The reason for this period will be described in the paper, as will the specific mechanism that underlies this behavior. Although there are great limitations in the possibility of tailoring these orbital variations by means of spacecraft maneuvers, it is interesting to note that this evolution appears likely to drive the MMS orbit into the outer cusps of the magnetosphere: this would be of great interest for the collection of novel science during a future phase of the extended mission.

## **OBSERVED EVOLUTION OF OVERALL MMS ORBIT GEOMETRY**

Before MMS raised its apogee radius from 12 to  $25 R_E$  during Phase 2a, the main change in orbital geometry was a slow secular drift in both right ascension of the ascending node (RAAN) and argument of perigee (AOP). Both of these effects were caused by the oblateness of the Earth. The inclination of the orbit was essentially constant, varying by only 0.3 deg over the two years since launch, as would be expected under oblateness alone. The semi-major axis of the orbit was also basically constant, as was its eccentricity: apogee and perigee radius were therefore essentially fixed also. However, once the spacecraft were partway through the Phase 2a apogee-raising campaign, the behavior of the orbit changed abruptly, almost as if a switch had been thrown. While semi-major axis remained virtually constant, eccentricity began varying considerably, causing apogee and perigee radius to oscillate in an equal and opposite fashion. This behavior necessitated two perigee-raise maneuvers, on Apr. 16 and Oct. 1, 2017, which raised perigee by 520-690 km and required the use of 10-13 kg of fuel, in order to keep the minimum altitude above the specified threshold of 700 km. (This limit was selected so as to prevent excessive damage to the tip mass probes from atomic oxygen, as well as to prevent close approaches to the many satellites in low Earth orbit.) In addition, the inclination of the orbit relative to both Equator and Ecliptic began a slow cyclic evolution, as did the elevation, or latitude, of the apogee vector out of either Ecliptic or Equator.

The reason for the new behavior of the orbit is of course the enhanced lunisolar effects that are experienced around the new higher apogee. It should be noted that both Sun and Moon have a significant

effect on the orbit: the solar effects are evident in oscillations with a period of 6 months (i.e. half the period of apparent solar motion relative to the Earth) and the lunar at a period of about two weeks (i.e. half the lunar orbit period). In the higher orbit, MMS can approach closer to the Moon than previously, but clearly does not approach closer to the Sun than hitherto. The enhanced solar effects on the orbit are therefore not a consequence of the solar perturbing accelerations becoming larger around apogee, but rather of the fact that the gravitational attraction of the Earth that they are being compared to is itself smaller around the new apogee. The fact that lunisolar perturbations “switched on” rather abruptly partway through the Phase 1 apogee-raise campaign, when semi-major axis was increased from 6.6 to 13.1  $R_E$ , is consistent with the *Laplace radius* of the Earth: this is the radius above which third-body perturbation effects overtake the oblateness perturbations that dominate for low orbits. For the Earth, and considering only solar perturbations for simplicity, the Laplace radius is found [7] to be 8.41  $R_E$ : this corresponds well with a semi-major axis midway through the Phase 2a apogee-raise campaign, with an apogee radius of 15.62  $R_E$ .

The following plots give in detail the actual evolution of the MMS orbit since launch, as well as its predicted behavior into the future, up to the point of expected reentry: if no further maneuvers are performed to delay it, this is predicted to occur in 2030. Fig. 1 shows semi-major axis and the apogee and perigee radii (all in  $R_E$ ) vs epoch. The fact that semi-major axis is nearly constant can be clearly seen, as can the equal and opposite oscillations in apogee and perigee radii that became more significant after the Phase 2a apogee-raise campaign. This variation in apogee and perigee radius is a consequence of variations in eccentricity, shown in Fig. 2. Fig. 3 then shows the evolution in perigee altitude: this includes the effects of the perigee-raise maneuvers that were carried out on Apr. 16 and Oct. 1, 2017. The increased perigee oscillations that occurred after Phase 2a in early 2017 can now be seen more clearly. An additional apogee-raise campaign, taking apogee radius from 25 to 29.34  $R_E$ , was carried out in Feb. 2019: see the companion paper [11]. The variations in perigee altitude can be seen to increase even further after this point, at first suggesting that this additional increase in apogee radius greatly increased perigee variability. However, Fig. 4 shows that this is not actually the case: this plot shows the evolution in perigee altitude if apogee radius remained at 25  $R_E$  indefinitely. In the two cases, the changes in perigee are certainly different, but the variability is large in either case. Note also that the overall period of the perigee evolution is a little over 6 years for the actual orbit, and slightly shorter if apogee radius were to remain at 25  $R_E$ . There is therefore a limited degree of controllability over when reentry will occur: for MMS, it can be brought earlier or later, in 6-year steps, by typically a fairly modest change in perigee altitude. However, it is not feasible to cause reentry to be delayed by, for instance, 3 or 9 years: the Sun and Moon are driving reentry epoch. This mechanism is also much more predictable than is reentry of a low Earth orbit satellite, where atmospheric drag can vary considerably and affect reentry time significantly. For a high-eccentricity orbit like that of MMS, the spacecraft typically only encounter drag on the final perigee pass, eliminating this source of unpredictability from the dynamics.

The orientation of the MMS orbit also evolves significantly under lunisolar effects, with an overall period roughly twice as long as that of perigee. Fig. 5 summarizes the motion of the orbit relative to the Equator by plotting the equatorial inclination, RAAN and AOP throughout the mission. The difference in the behavior prior to and after the Phase 2a apogee-raising can clearly be seen. It can also be seen that the MMS orbit, which was launched due East from Kennedy Space Center into an equatorial inclination of 28.7 deg, came within a few degrees of equatorial in early 2019. This necessitated additional vigilance to check for close approaches with geosynchronous satellites during this period; there was only one, in late 2018, at a fairly high miss distance of about 18 km.

Fig. 6 then gives the equivalent angles defined relative to the Ecliptic: since MMS is a heliophysics science mission, these quantities are of great interest. So too is the position of the MMS apogee vector relative to the Ecliptic, as the bulk of MMS science is carried out in the region around apogee. Fig. 7 shows the azimuth of the projection of apogee into the Ecliptic throughout the mission, as well as a

“dogleg” angle, RAAN plus AOP, that is sometimes used as a simplified proxy for this azimuth. The slow increase in these angles over time implies that MMS takes slightly over one year to make one complete revolution relative to the Earth-Sun line: this additional time can be shown to be 2.94 days, on average, for each year of the remaining extended mission. Fig. 8 then plots the elevation of the MMS apogee vector out of the Ecliptic (this angle can also be termed the ecliptic latitude), as well as the ecliptic latitudes of points at a radius of  $11 R_E$  on the ascending and descending flanks of the orbit. The increasing oscillations in these angles imply that the orbit around apogee will sample higher latitudes as the extended mission progresses, potentially leading to new types of science observations, for instance of the outer cusp of the magnetosphere [12].

It is clear from these plots that certain of the orbital variables, notably eccentricity (and hence apogee and perigee radii) and ecliptic inclination vary on a cycle of roughly 6 years; others, for instance the ecliptic latitude of apogee, repeat over a cycle twice as long, or approximately 13 years. These repeat cycles can be explained by examining the interval between successive repetitions of the same relative geometry of Sun, Moon and the MMS orbit (specifically its apogee direction, a key factor for the highly eccentric MMS orbit). As noted above, the MMS orbit takes roughly 368.20 days to perform a complete revolution relative to the Earth-Sun line. At this point, MMS and Sun will be in the same configuration relative to the Earth; however, they will have rotated 2.9 deg relative to the fixed stars from the start of one “MMS year” to the next. Since the Moon takes 0.22 days to cover this additional angle, if the complete Sun-Moon-MMS apogee geometry is to repeat after  $N$  “MMS years”, for  $N$  some integer, this interval must be equal to  $M$  lunar sidereal periods plus  $0.22N$  days, for  $M$  also an integer. By examination of all possible values for the integers  $N$  and  $M$ , it is found that the Sun-Moon-MMS apogee geometry repeats, to a close approximation, after 13 years, or 175 lunar sidereal periods. This is consistent with the results seen in the plots.

Note also that, if the recent apogee-raise had not been performed and apogee radius had remained at  $25 R_E$ , simulations showed that the resulting repeat cycle would be 12 rather than 13 years. This lower orbit had a slightly higher annual inertial drift for the projection of apogee into the Ecliptic, as a result of a somewhat higher oblateness-induced nodal regression rate. Taking a value for this annual drift of 3.6 rather than 2.9 deg and performing the same analysis as summarized here, a repetition cycle of 12 years is indeed obtained.

The preceding plots have summarized the evolution of the MMS orbit, emphasizing the difference in behavior between the oblateness-dominated Phase 1 of the mission and the lunisolar-dominated Phases 2b and beyond. The next section will endeavor to explain the reasons behind the salient features of this lunisolar-dominated evolution. As part of this discussion, the reason why the 13-year repetition cycle is halved to about 6 years for a subset of the orbital variables will also be addressed.

## UNDERLYING LUNISOLAR EFFECTS ON MMS ORBIT

The Lidov-Kozai mechanism [7] describes the evolution of an orbit of a satellite that is significantly perturbed by the gravitational attraction of a third body. It has recently proved very useful in the study of systems of exoplanets, where the orbit of one planet can be affected significantly by the gravitational attraction of the others, even to the extent of being “flipped” to become retrograde. Note that the Lidov-Kozai mechanism is often referred to simply as the Kozai mechanism, although Lidov’s initial paper on the subject [9] predated that of Kozai [10]. The publication by Lidov described his work in relation to the Luna 3 spacecraft, launched on October 4, 1959 (two years to the day after the launch of Sputnik 1), which flew in a highly elliptical Earth orbit past the Moon, took the first images of the far side, downlinked them on the way down to perigee, and then reentered in April 1960, after 11 revs, as a result

of lunisolar perturbations. Since this paper was written in Russian, it does not appear to have received widespread attention at the time.

Although the Lidov-Kozai mechanism describes the motion in response to a single perturbing body and MMS is affected by both Sun and Moon, the theory still applies well to this case. This is largely a result of the fortunate fact that the orbital plane of the Moon is nearly coincident with that of the Earth around the Sun: the lunar ecliptic inclination is only 5.145 deg. A key quantity in Lidov-Kozai theory is the geometry of the satellite orbit relative to the plane of the orbit of the perturber, so the Ecliptic can reasonably be used for both Sun and Moon in such studies.

Double-averaging of the circular restricted three-body problem [7] reveals that there are three constants of the motion,  $\{c_i, i=0,1,2\}$ , associated with the Lidov-Kozai Hamiltonian [9][10]. These are:

(1) *Semi-major axis:*

$$c_0 = a. \tag{1}$$

Since the total mechanical energy of the satellite depends only on semi-major axis, it therefore is also conserved.

(2) *Component of angular momentum normal to the Ecliptic:*

The magnitude of the angular momentum of the satellite orbit is given as  $h = \sqrt{\mu p} = \sqrt{\mu a(1-e^2)}$ . Its component normal to the Ecliptic is  $h_{ecl\_perp} = h \cos i_{ecl}$ : squaring this gives  $h_{ecl\_perp}^2 = \mu a(1-e^2) \cos^2 i_{ecl} \propto (1-e^2) \cos^2 i_{ecl}$ , since the semi-major axis is constant. The corresponding dimensionless constant of the motion can therefore be written as

$$c_1 = (1-e^2) \cos^2 i_{ecl}. \tag{2}$$

Note that, since the orbit of the Moon is only approximately coplanar with the Ecliptic, this conservation law is only approximately true for satellites in high Earth orbits that are affected by both Sun and Moon. It is, however, a close approximation. It should also be noted that  $c_1$  is one of the three *Delaunay variables* of the system; another depends only on semi-major axis. All three are conserved in the two-body problem, but only these two are in the circular restricted three-body problem: the third, the total angular momentum, is not.

(3) *Lidov-Kozai Hamiltonian:*

This can be shown [7] to reduce to

$$c_2 = e^2 \left\{ \frac{2}{5} - \sin^2 i_{ecl} \sin^2 \omega_{ecl} \right\}. \tag{3}$$

Fig. 9 plot the first of these constants of the motion, the semi-major axis, for MMS from launch to predicted reentry. Fig. 10 then shows the dimensionless constant  $c_1$  throughout the mission. It can be seen that this is approximately constant, as expected. Indeed, it varies far less than does the total angular momentum of the orbit, as is demonstrated by Fig. 11, where these quantities are plotted together. The

final Lidov-Kozai constant  $c_2$  is then shown in Fig. 12: this again has an approximately fixed value over the mission once apogee radius has been raised to its current value.

It can be seen from Eq. (2) that the eccentricity and ecliptic inclination of the MMS orbit must vary in a coordinated fashion under lunisolar perturbations. This is further demonstrated by Fig. 13, where these two orbital elements are plotted over the course of the mission: their high correlation can clearly be seen. The fact that eccentricity experiences significant variations is, as has already been noted, the mechanism by which lunisolar effects can lead to eventual reentry of the satellite. Since eccentricity can be expressed as

$$e = \sqrt{1 + \frac{2Eh^2}{\mu^2}}, \quad (4)$$

and the semi-major axis, and hence energy  $E$ , are essentially constant, the observed variations in eccentricity must result from the changes in the total angular momentum  $h$  that were shown in Fig. 11. (Since  $E$  is negative, any increase in  $h$  will lead to a decrease in  $e$ , and hence to an increase in perigee radius.) The next section will give a physical description of the way in which these changes in angular momentum actually arise.

## LUNISOLAR-INDUCED CHANGES IN ANGULAR MOMENTUM

Fig. 14 is a sketch of the relative geometry of Earth, Sun and MMS. Of course, this diagram is not to scale: the distance from Earth to spacecraft is in reality much less than that from Sun to either Earth or MMS. The net solar perturbation acceleration on the spacecraft is given as the difference between that acting on MMS and that acting on the Earth:

$$\mathbf{a}_{Sun} = \left( \frac{\mu_{Sun}}{r_{Sun/sat}^3} \right) \mathbf{r}_{Sun/sat} - \left( \frac{\mu_{Sun}}{r_{Sun}^3} \right) \mathbf{r}_{Sun}. \quad (5)$$

Since  $r_{Sun/sat} \approx r_{Sun}$ , a binomial expansion can be used to express  $r_{Sun/sat}^{-3}$  in terms of  $r_{Sun}^{-3}$  so as to simplify this acceleration expression. Specifically,

$$\begin{aligned} r_{Sun/sat}^{-3} &= (r_{Sun/sat}^2)^{-1.5} = (\mathbf{r}_{Sun/sat}^T \mathbf{r}_{Sun/sat})^{-1.5} = ([\mathbf{r}_{Sun} - \mathbf{r}_{sat}]^T [\mathbf{r}_{Sun} - \mathbf{r}_{sat}])^{-1.5} \\ &\approx (\mathbf{r}_{Sun}^T \mathbf{r}_{Sun} - 2\mathbf{r}_{Sun}^T \mathbf{r}_{sat})^{-1.5} = (r_{Sun}^2 - 2\mathbf{r}_{Sun}^T \mathbf{r}_{sat})^{-1.5} \\ &= r_{Sun}^{-3} \left\{ 1 - \left( \frac{2}{r_{Sun}^2} \right) \mathbf{r}_{Sun}^T \mathbf{r}_{sat} \right\}^{-1.5} \approx r_{Sun}^{-3} \left\{ 1 + \left( \frac{3}{r_{Sun}^2} \right) \mathbf{r}_{Sun}^T \mathbf{r}_{sat} \right\}^{-1.5}. \end{aligned} \quad (6)$$

The net solar acceleration on the spacecraft then becomes, to first order in the small quantity  $r_{sat}/r_{Sun}$ ,

$$\mathbf{a}_{Sun} \approx \left( \frac{\mu_{Sun}}{r_{Sun}^3} \right) r_{sat} \left\{ 3\cos\alpha \hat{\mathbf{r}}_{Sun} - \hat{\mathbf{r}}_{sat} \right\}, \quad (7)$$

where  $\alpha$  is the angle between  $\mathbf{r}_{Sun}$  and  $\mathbf{r}_{sat}$  and  $\hat{\cdot}$  denotes a unit vector.

The rate of change of total orbital angular momentum that is produced by this perturbing acceleration is equal to its torque about the center of the Earth,  $\boldsymbol{\tau}_{solar} = \mathbf{r}_{sat} \times \mathbf{a}_{Sun} (= r_{sat} \hat{\mathbf{r}}_{sat} \times \mathbf{a}_{Sun})$ . The second term in Eq. (7) clearly does not contribute to this cross product, giving

$$\boldsymbol{\tau}_{solar} \approx \left( \frac{\mu_{Sun}}{r_{Sun}^3} \right) r_{sat}^2 \left\{ 3 \cos \alpha (\hat{\mathbf{r}}_{sat} \times \hat{\mathbf{r}}_{Sun}) \right\}. \quad (8)$$

This torque vector must necessarily be normal to the Sun vector  $\hat{\mathbf{r}}_{Sun}$ , also denoted by  $\hat{\mathbf{x}}_{GSE}$  in the GSE coordinate frame. (This frame rotates once per year and has  $\hat{\mathbf{x}}_{GSE}$  along the Earth-Sun line,  $\hat{\mathbf{y}}_{GSE}$  in the Ecliptic and rotated 90 deg from  $\hat{\mathbf{x}}_{GSE}$  in the direction of motion if the Earth, and  $\hat{\mathbf{z}}_{GSE}$  directed along the Ecliptic normal.) The solar perturbation torque must therefore lie in the  $(\hat{\mathbf{y}}_{GSE}, \hat{\mathbf{z}}_{GSE})$ -frame. But the constant of the motion  $c_1$  of Eq. (2) is just the component of orbital angular momentum along  $\hat{\mathbf{z}}_{GSE}$ : changes in this component must therefore average to zero. The only significant net changes in angular momentum produced by solar perturbations are consequently along the  $\hat{\mathbf{y}}_{GSE}$  axis. In other words, the angular momentum vector rocks back and forth about the Sun line as a result of solar perturbations.

Note that an analogous expression to Eq. (7) can be derived for the lunar perturbations. Of course, the Earth-Moon vector which the lunar perturbing torque must be perpendicular to rotates faster than does the Earth-Sun vector  $\hat{\mathbf{x}}_{GSE}$ : the lunar torque will therefore tend to average out more nearly to zero over an extended period than does the solar torque. Studying Eq. (8) thus gives a good general understanding of the effects of lunisolar perturbations on the MMS orbit. (Another point to bear in mind for lunar perturbations is that the Earth-Moon distance is typically less than an order of magnitude greater than the Earth-MMS distance: the second-order term in the binomial expansion Eq. (6) must therefore also be included. However, it can be shown [2] that the contribution of this term averages to zero over the course of a lunar orbit. The resulting expression for the net lunar acceleration on MMS is thus entirely analogous to Eq. (7), and that for the resulting torque to Eq. (8).)

So, lunisolar perturbations cause the MMS orbit normal to rock relative to the Ecliptic at the 13-year period that was previously discussed, first to one side and then to the other. This causes the ecliptic inclination of the orbit to vary over roughly a 6-year cycle: this is seen in Fig. 6. The peak values of ecliptic inclination in 2021 and 2027 correspond to points where the angular momentum vector is tipped as far as possible away from the Ecliptic normal. At such times, since the component of angular momentum along the Ecliptic normal is constant, it follows that the magnitude of the angular momentum vector,  $h$ , must be as large as possible: see Fig. 11. Thus, as discussed following Eq. (4), perigee radius must also follow the same roughly 6-year cycle, reaching maximum values in 2021 and 2027: this is evident in Figs. 1 and 3. The evolution of perigee radius and orbital orientation is therefore inextricably linked, confirming the conclusions of Fig. 13.

It can be seen from this discussion that the evolution of an orbit such as that of MMS under lunisolar perturbations is highly constrained: not only must the three constants of the motion given by Eqs. (1)-(3) be essentially fixed, but the periodicity of the resulting motion is defined from the geometry of Sun, Moon and satellite. There is therefore little scope for greatly altering the resulting behavior by means of spacecraft maneuvers. This has been seen for the case of MMS: even quite a significant increase in

apogee radius, from 25 to 29.34  $R_E$ , did not alter the subsequent evolution of the orbit in a major way. In particular, while it is certainly possible to prevent reentry at some given dip in the perigee altitude by carrying out a perigee-raise burn, it is not realistic to greatly alter the approximate 6-year perigee cycle seen in Fig. 3, or to move a minimum forward or back by several years. Basically, once a satellite is inserted into an orbit that is strongly subject to lunisolar effects, its future behavior is, to a large extent (although not totally), pre-defined.

## CONCLUSIONS

This paper has described the significant variations in the geometry of the highly eccentric MMS orbit that occur as a result of the gravitational attraction of both Sun and Moon. The MMS apogee radius is now 29.34 Earth radii, or virtually halfway to the Moon, so these third-body effects are by far the most significant source of orbital perturbations. One of their key consequences is an oscillation in perigee altitude on an approximately 6 year cycle. This variation has already required perigee-raise maneuvers to avoid an untimely reentry, and will drive the eventual demise of the spacecraft. There is also a long-term evolution in the orientation of the MMS orbit, with period roughly twice as long. This effect looks likely to be useful for MMS science studies, as it will bring the spacecraft into new regions of the magnetosphere, for instance the outer polar cusps. So, even though this evolution to a large extent cannot be controlled by maneuvers, it can still be taken advantage of for the benefit of the mission.

## ACKNOWLEDGEMENTS

The authors wish to acknowledge the invaluable contributions of the additional members of the MMS flight dynamics team and of the MMS flight operations team.

## REFERENCES

- [1] A.S. Sharma and S.A. Curtis, "Magnetospheric Multiscale Mission", *Nonequilibrium Phenomena in Plasmas*, Astrophysics and Space Science Library Vol. 321, Springer-Netherlands. pp. 179–195, 2005.
- [2] T. Williams, "Launch Window Analysis for the Magnetospheric Multiscale Mission", Paper AAS12-255, AAS/AIAA Space Flight Mechanics Meeting, Charleston, SC, Jan./Feb. 2013.
- [3] T. Williams, N. Ottenstein, E. Palmer and M. Farahmand, "Initial Satellite Formation Flight Results from the Magnetospheric Multiscale Mission", Paper AIAA 2016-5505, AIAA SPACE-2016, Long Beach, CA, Sept. 2016.
- [4] T. Williams, N. Ottenstein, E. Palmer and D. Godine, "Satellite Formation Flight Results from Phase 1 of the Magnetospheric Multiscale Mission", International Workshop on Satellite Constellations and Formation Flying, Boulder, CO, June 2017.
- [5] T. Williams, N. Ottenstein, E. Palmer and J. Hollister, "Results of the Apogee-Raising Campaign of the Magnetospheric Multiscale Mission", Paper AAS 17-760, AAS/AIAA Astrodynamics Specialist Conference, Stevenson, WA, Aug. 2017.
- [6] D.H. Fairfield, "A Statistical Determination of the Shape and Position of the Geomagnetic Neutral Sheet", *J. Geophysical Research*, Vol. 85, No. A2, pp. 775-780, Feb. 1980.
- [7] I.I. Shevchenko, *The Lidov-Kozai Effect – Applications in Exoplanet Research and Dynamical Astronomy*, Springer, 2017.
- [8] R.L. Lin, X.X. Zhang, S.Q. Liu, Y.L. Wang and J.C. Gong, "A Three-Dimensional Asymmetric Magnetopause Model", *J. Geophysical Research*, Vol. 115, No. A04207, pp. 1-12, Apr. 2010.
- [9] M.L. Lidov, "Evolution of artificial planetary satellites under the action of gravitational perturbations due to external bodies", *Artificial Satellites of the Earth*, Vol. 8, pp. 5-45, 1961 (in Russian).
- [10] Y. Kozai, "Secular perturbations of asteroids with high inclination and eccentricity", *Astron. J.*, Vol. 67, pp. 591-598, 1962.

- [11] T. Williams, E. Palmer, D. Godine, J. Hollister, N. Ottenstein and B. Vint, “MMS Extended Mission Eclipse Mitigation and Solar Wind Turbulence Science Campaign”, AAS/AIAA Astrodynamics Specialist Conference, Portland, ME, Aug. 2019.
- [12] T.A. Fritz and S.F. Hung (ed.), *The Magnetospheric Cusps: Structure and Dynamics*, Springer, The Netherlands, 2005.

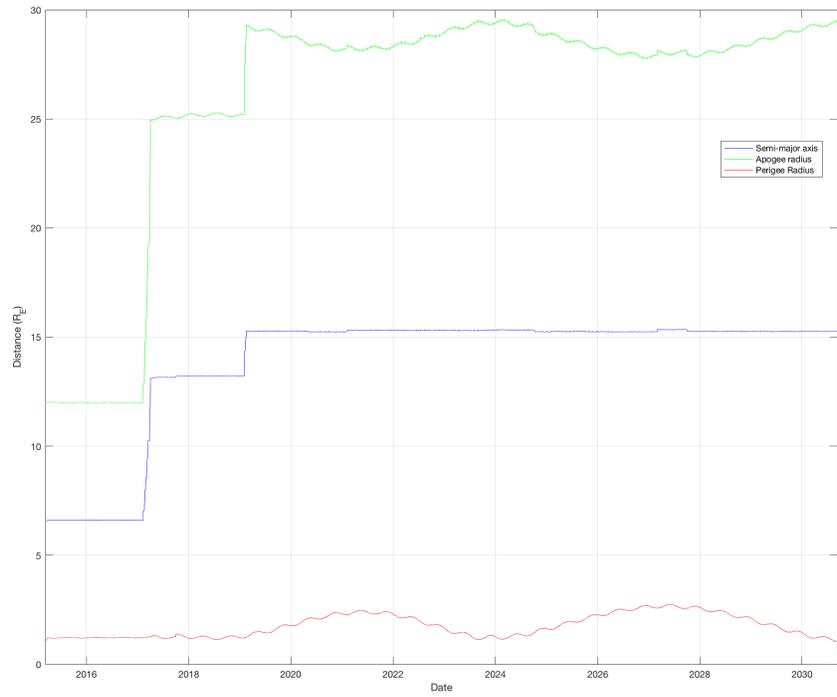


**Figure 1. Evolution of semi-major axis and apogee and perigee radii throughout mission.**

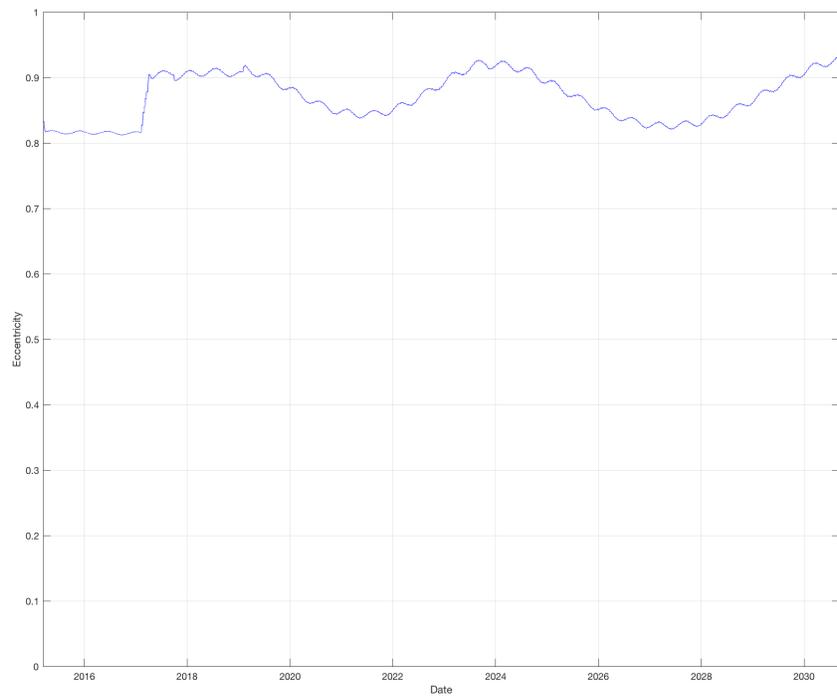


**Figure 2. Evolution of eccentricity throughout mission.**

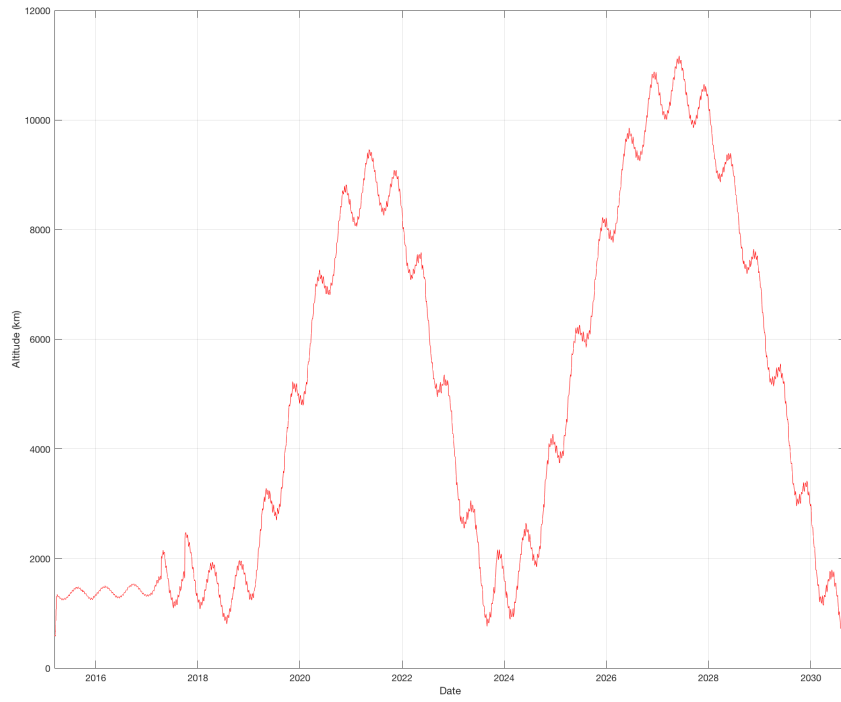


**Figure 3. Evolution of perigee altitude throughout mission.**

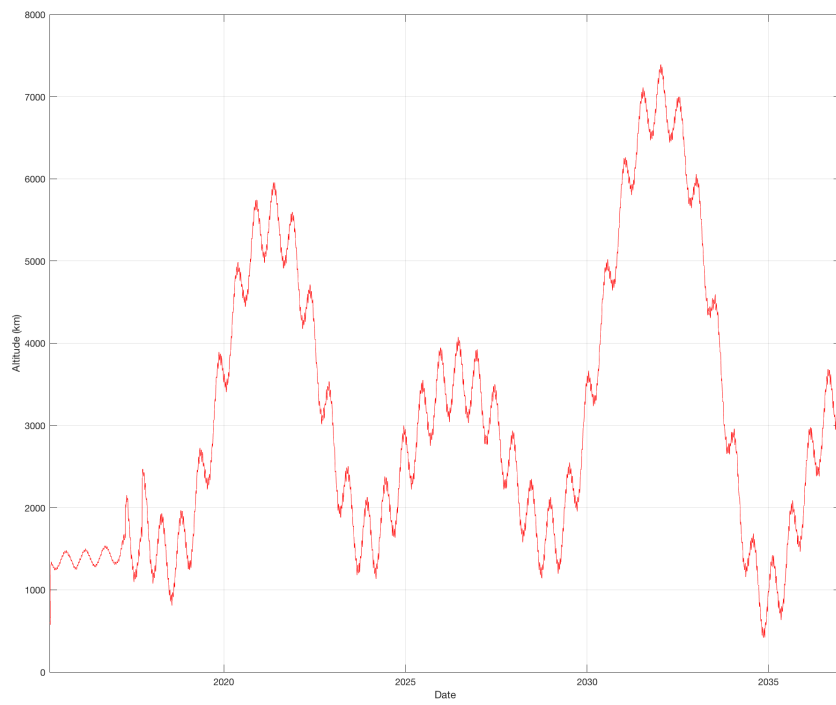


**Figure 4. Evolution of perigee altitude if apogee radius held at  $25 R_E$ .**

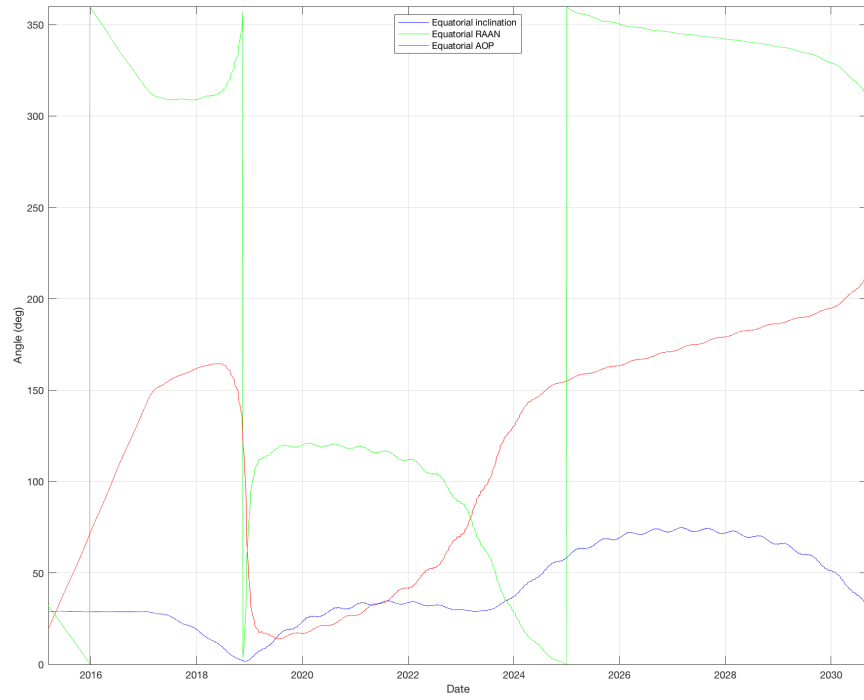


**Figure 5. Evolution of equatorial inclination, RAAN and AOP throughout mission.**

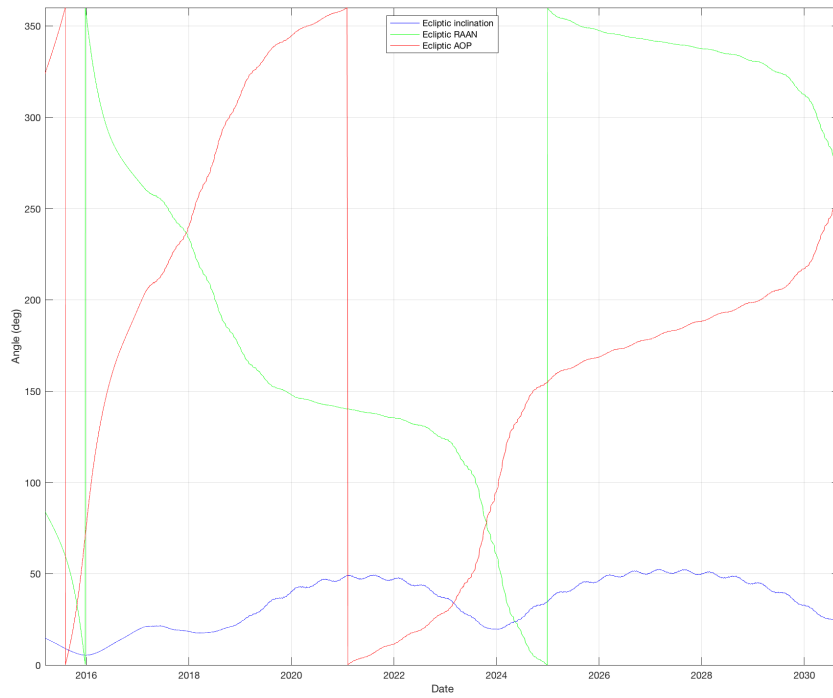


**Figure 6. Evolution of ecliptic inclination, RAAN and AOP throughout mission.**

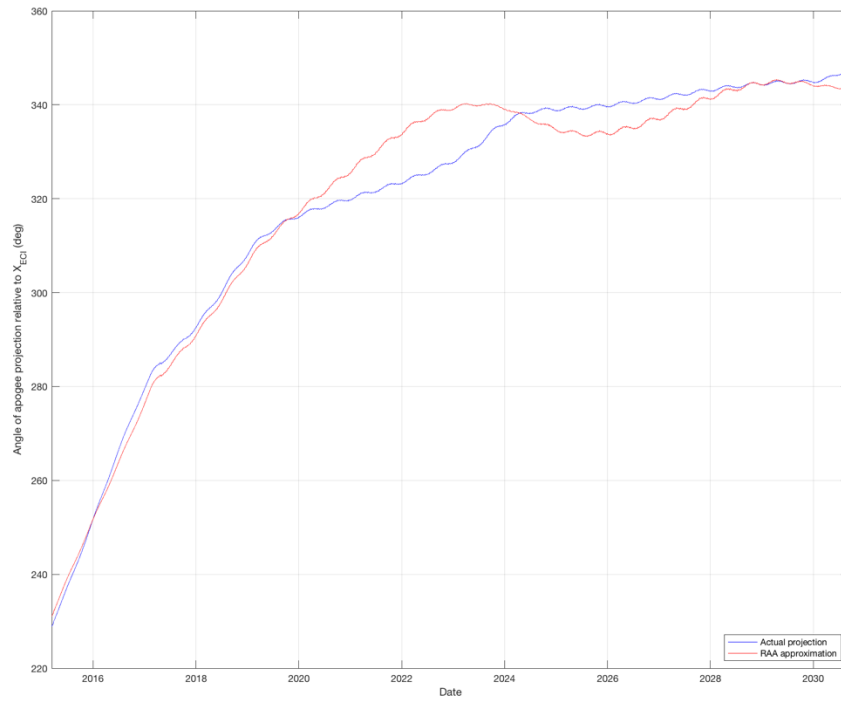


**Figure 7. Evolution of inertial azimuth of apogee vector projected onto Ecliptic.**

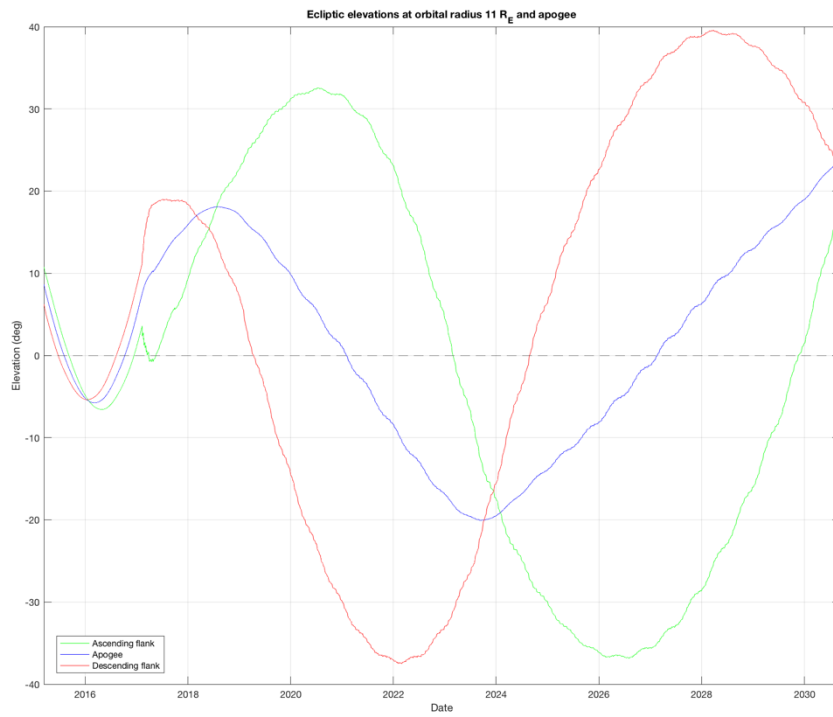


**Figure 8. Evolution of ecliptic latitude of apogee and  $11 R_E$  flank vectors throughout mission.**

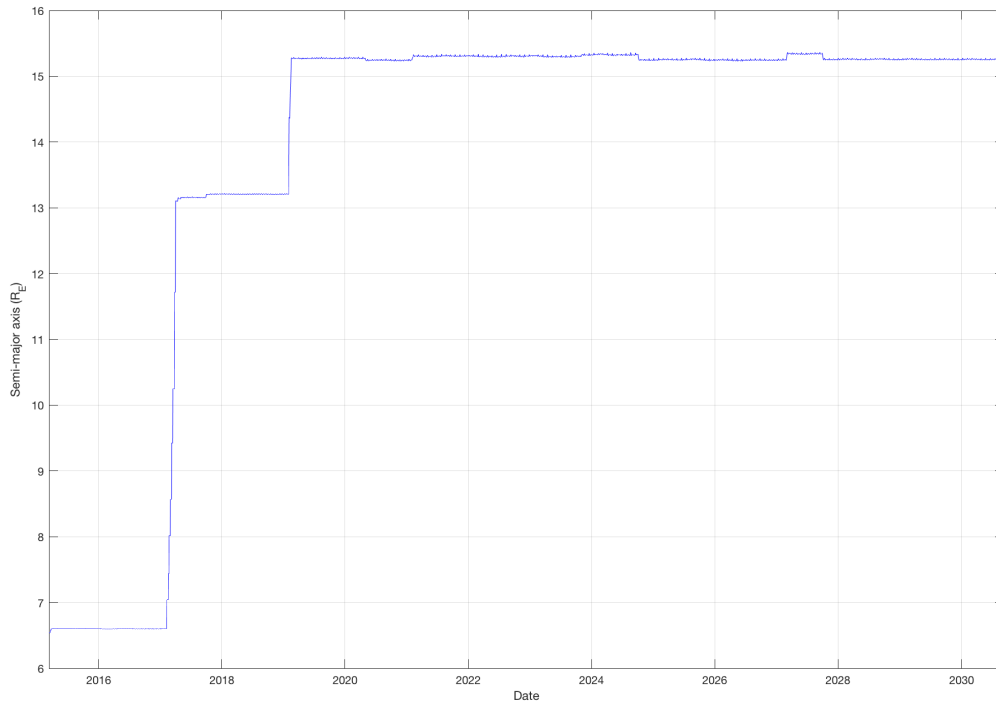


**Figure 9. Evolution of Lidov-Kozai constant  $c_0$  (SMA) throughout mission.**

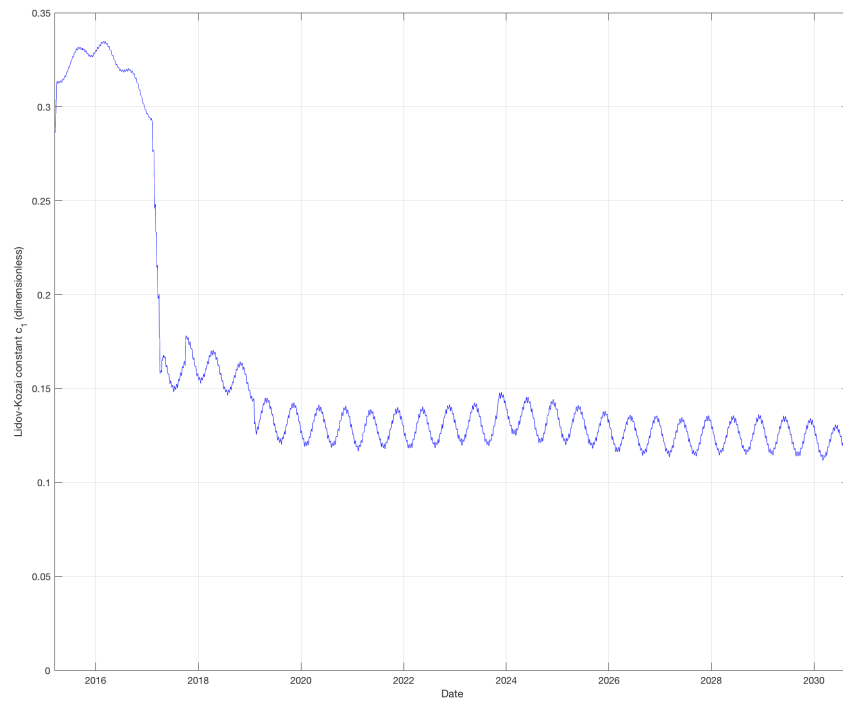


**Figure 10. Evolution of Lidov-Kozai constant  $c_1$  throughout mission.**

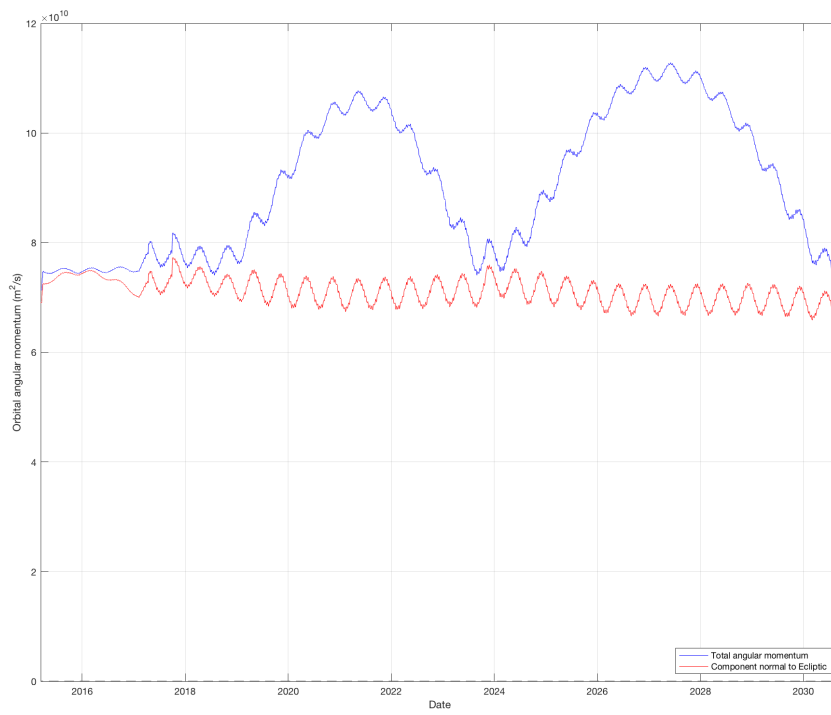


**Figure 11. Evolution of total angular momentum and its component normal to Ecliptic.**

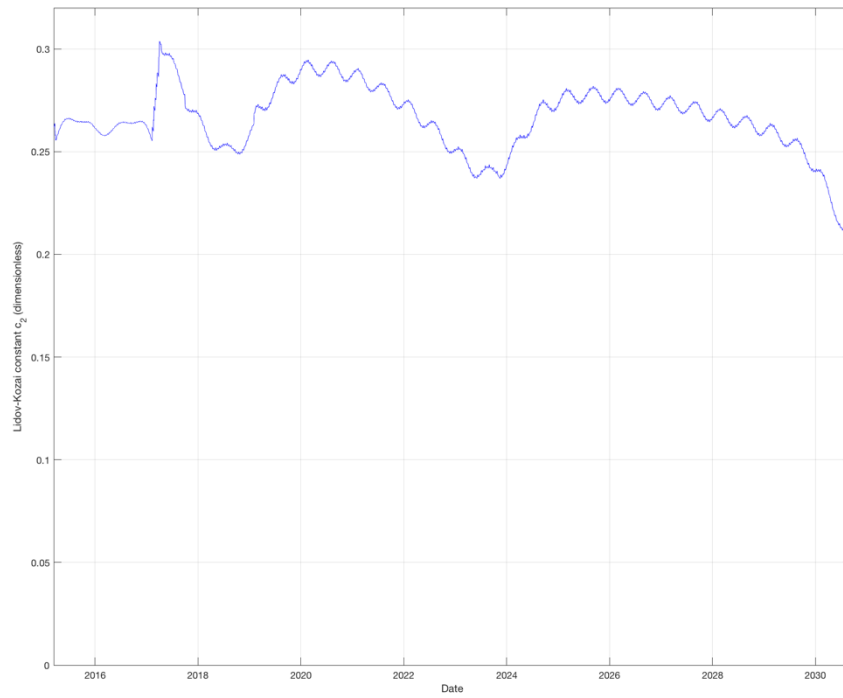


**Figure 12. Evolution of Lidov-Kozai constant  $c_2$  throughout mission.**

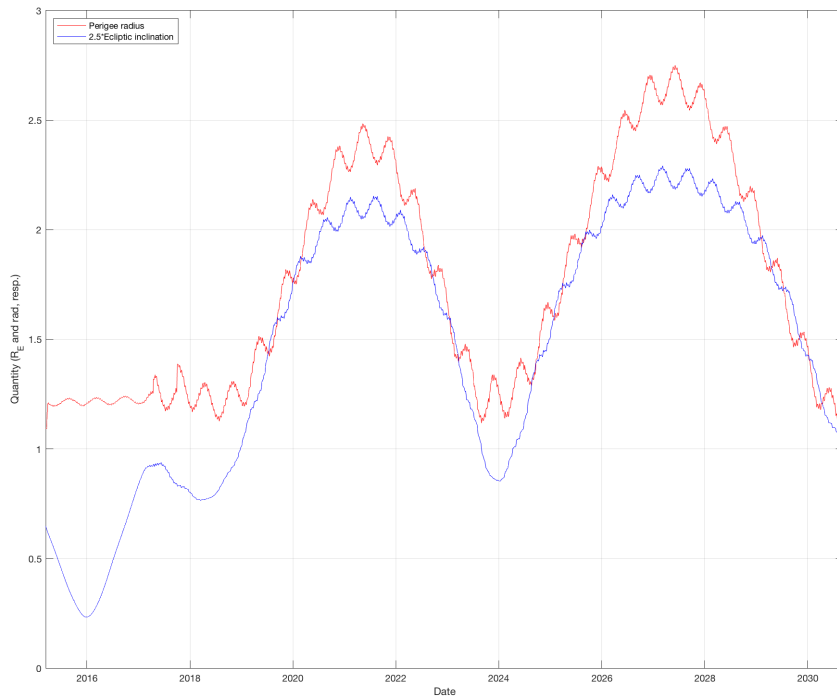


**Figure 13. Evolution of ecliptic inclination and perigee radius throughout mission.**

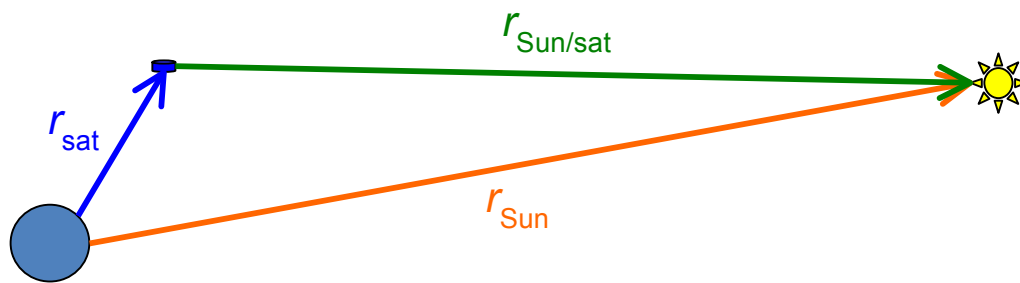


**Figure 14. Relative geometry of Sun, Earth and spacecraft.**